Journal of Alloys and Compounds 831 (2020) 154921

Contents lists available at ScienceDirect

Journal of Alloys and Compounds

journal homepage: http://www.elsevier.com/locate/jalcom

One-step solvothermal synthesis of mixed nickel–cobalt sulfides as high-performance supercapacitor electrode materials

To Van Nguyen [a, *], Luong Trung Son [a], Pham Manh Thao [a], Le The Son [a], Doan Tien Phat [a], Ngo Thi Lan [a], Nguyen Van Nghia [b, c], Tran Viet Thu [d, **]

[a] Department of Chemical Engineering, Le Quy Don Technical University, 236 Hoang Quoc Viet, Hanoi, 100000, Viet Nam
[b] Research Center of Advanced Materials and Applications, Institute of Architecture, Construction, Urban and Technology, Hanoi Architectural University, Hanoi, 100000, Viet Nam
[c] Department of Physics, Open Training Institute, Hanoi Architectural University, Hanoi, 100000, Viet Nam
[d] Institute of Research and Development, Duy Tan University, K7/25 Quang Trung, Danang, 550000, Viet Nam

ARTICLE INFO

Article history:
Received 7 January 2020
Received in revised form
22 March 2020
Accepted 23 March 2020
Available online 24 March 2020

Keywords:
Solvothermal synthesis
Mixed nickel-cobalt sulfides
High specific capacitance
Supercapacitor
Synergistic effect

ABSTRACT

In this work, mixed nickel-cobalt sulfides (NCSs) were prepared by a facile solvothermal method. Structural and morphological characterization of synthesized materials were confirmed by X-ray diffractometry, X-ray photoelectron spectroscopy, scanning and transmission electron microscopy. Electrochemical measurements revealed that mixed NCSs exhibit pseudocapacitor behaviour and their capacitance was strongly dependent on the composition. Interestingly, the electrochemical performance of the mixed NCSs has been significantly improved in comparison to the pristine nickel sulfide or cobalt sulfide. Particularly, the mixed NCS prepared at a nickel:cobalt molar ratio of 3:1 exhibited a specific capacitance of 2599.6 F g^{-1} at a scan rate of 10 mV s^{-1} (or 1345 F g^{-1} at a current density of 2 A g^{-1}) and retained 95% of its initial capacitance after 3000 charge-discharge cycles. The excellent electrochemical performances of NCSs indicate they are promising candidate for supercapacitor electrode.

1. Introduction

Over the past few decades, the increasing demand for portable electronic devices and electric vehicles has set higher requirements for power sources such as high durability, safe to use, compact, and lightweight. To resolve this problem, supercapacitors and batteries are among the most promising candidates selected to research and develop. In comparison with batteries, supercapacitors are receiving more intense attention because they have several advantages such as simple configuration, long cycle stability, high coulombic efficiency and fast charging-discharging rates [1–3]. Based on charge storage mechanisms, SCs are generally classified into two types: electrochemical double-layer capacitors (EDLCs) and Faradaic redox reaction pseudocapacitors (PCs) [4–6].

EDLC stores electrical energy based solely on the absorption and desorption of the electrolyte ions at the electrolyte/electrode interface. EDLC electrode materials are largely based on carbon materials with large surface area such as activated carbon [7], carbon foam [8], carbon nanotubes [9], and graphene [9–11]. Meanwhile, PCs operate based on redox reactions between a thin layer of active electrode materials and electrolyte ions at their interface [12]. Therefore, typical electrode materials used in PCs are transition metal oxides with multiple oxidation states such as MnO_2 [13,14], $NiCo_2O_4$ [15–17], and $MnFe_2O_4$ [11]. PCs generally provide higher energy density than EDCLs but suffer from lower power density due to poor electrical conductivity. Supercapacitors using transition metal oxides as electrode materials have slow charge and discharge rate [18–20].

Recently, metal sulfides have received great attention as a promising electrode materials for pseudocapacitor because of their high specific capacitance, high electron conductivity abundance, low cost, and environmental friendliness [21,22]. It has been reported that CoS_2 octahedrons directly applied as electrodes for supercapacitors show typical pseudocapative properties with maximum specific capacitance of 236.5 F g^{-1} at 1 A g^{-1} [23]. In addition, NiS_2 nanomaterial prepared by microwave assisted method and used as an electrode material for supercapacitor

* Corresponding author.
** Corresponding author.
E-mail addresses: tptnhv@gmail.com (T.V. Nguyen), tranvietthu1@duytan.edu.vn (T.V. Thu).

https://doi.org/10.1016/j.jallcom.2020.154921
0925-8388/

delivers a specific capacitance of 695 F g^{-1} at 1.25 A g^{-1} [24]. Those studies indicated that, although individual nickel or cobalt sulfide electrodes possess high electron conductivity but their capacity is still lower than that of metal oxides materials. Several studies attacking this problem has mainly focused on combining different metal sulfides [25–27] or coupling metal sulfide with carbon-based materials or conducting polymers [28,29]. However, the effect of composition of mixed-metal sulfides on their electrochemical properties has not been extensively explored, in spite of their fundamental importance.

In this work, we report a facile simple solvothermal treatment route to prepare mixed nickel-cobalt sulfide (NCSs) with controlled nickel:cobalt (Ni:Co) molar ratios. The mixed NCSs is supposed to offer a synergistic effect contributed by NiS_2 and CoS_2. We also investigated the correlation between the composition, structure and electrochemical performance of the as-prepared mixed NCSs, which would be the valuable information to prepare other related metal sulfies systems for supercapacitor application. We found that all of the mixed NCSs display pseudocapacitive behaviour and their pseudocapacitances are strongly dependent on their composition. In particular, mixed NCS prepared at a Ni:Co molar ratio of 3:1 exhibited an enhanced C_s compared to those of pristine nickel or cobalt sulfide, indicating a synergistic effect of nickel and cobalt in all mixed NCSs.

2. Experimental

2.1. Chemicals

Nickel chloride hexahydrate ($NiCl_2 \cdot 6H_2O$), cobalt (II) chloride hexahydrate ($CoCl_2 \cdot 6H_2O$), sodium thiosulfate pentahydrate ($Na_2S_2O_3 \cdot 5H_2O$), ethylene glycol (EG), hydrochloric acid (HCl), Ni foam, acetylene black (AB), poly(vinylidene fluoride) (PVDF), N-methyl pyrrolidone (NMP). All the chemicals were of analytical grade and used without further purification, and were purchased from Shanghai Aladdin Bio-Chem Technology Co., Ltd. De-ionized (DI) water was used to prepare solutions in all experiments.

Table 1
Ratio between precursor chemicals for different samples.

	Amount (mmol)			
	$NiCl_2 \cdot 6H_2O$	$CoCl_2 \cdot 6H_2O$	$Na_2S_2O_3 \cdot 5H_2O$	Total
NS	10	0	15	25
NCS1	7.5	2.5	15	25
NCS2	5	5	15	25
NCS3	2.5	7.5	15	25
CS	0	10	15	25

2.2. Materials synthesis

All materials were synthesized via solvothermal process (Fig. 1). In a typical procedure, 15 mmol of $Na_2S_2O_3 \cdot 5H_2O$ and predetermined amounts of M^{2+} salts (M = Ni, Co) were dissolved into 150 ml of mixed ethylene glycol/water (ratio volume 1: 2) by magnetic stirring for 30 min, resulting in the formation of a pinkish solution. The total amount of M^{2+} salts was fixed at 10 mmol, where Ni:Co molar ratio was varied: 10/0 (NS); 7.5/2.5 (NCS1); 5/5 (NCS2); 2.5/7.5 (NCS3) and 0/10 (CS). The resulted mixture was transferred to a 200-ml Teflon-lined autoclave and heated to 160 °C for 10 h. After it was cooled down to room temperature, the product was washed with DI water and ethanol several times and dried at 60 °C in vacuum for 6 h. The precursor ratios and sample names are given in Table 1.

2.3. Material characterization

Characterization of all mixed metal sulfides were confirmed by X-ray diffraction (XRD, Siemens D5005 X-ray diffract meter with Cu-Kα radiation); thermal gravimetric analysis (TGA, PerkinElmer Pyris 6); scanning electron microscopy and energy-dispersive X-ray spectroscopy (SEM-EDS, JEOL JSM-6490 scanning electron

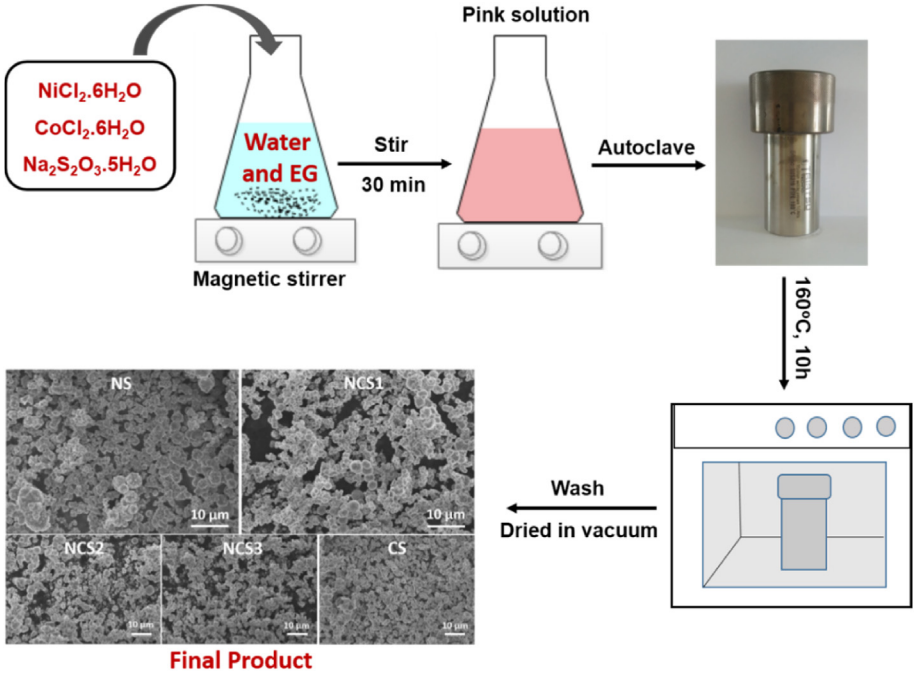

Fig. 1. Synthesis flowchart of NS, CS and mixed NCSs.

microscope); and transmission electron microscopy (TEM, JEOL JEM-1010).

2.4. Electrochemical measurements

To evaluate electrochemical properties of synthesized materials, we used cyclic voltammetry (CV), galvanostatic charge-discharge (GCD) and electrochemical impedance spectroscopy (EIS) measurements. All above measurements were performed on Metrohm Autolab PGSTAT 302 N with standard three-electrode system: working electrode, reference electrode (Ag/AgCl in 3 M KCl solution), counter electrode (Pt, sheet) and 3 M KOH aqueous solution as the electrolyte. To prepared working electrode, active material was mixed with acetylene black and PVDF (weight ratio 80:10:10) in a small amount of NMP solvent to make a homogeneous slurry. Then, 20 μL of homogeneous slurry were dropped onto Ni foam (0.25 cm × 0.25 cm) and dried in a vacuum heater at 60 °C for 2 h. The mass loading of active materials was about 0.64 mg cm^{-2}. Specific capacitance (C_s) of materials were calculated from CV and GCD curves using the formula $C_s = (\int I\,dt)/(m\,\Delta E)$, $C_s = (I\,\Delta t)/(m\,\Delta E)$, respectively, where I is the discharge current (A), Δt is discharge time (sec), ΔE is the potential window (V), and m is the weight of active material in the electrode (g).

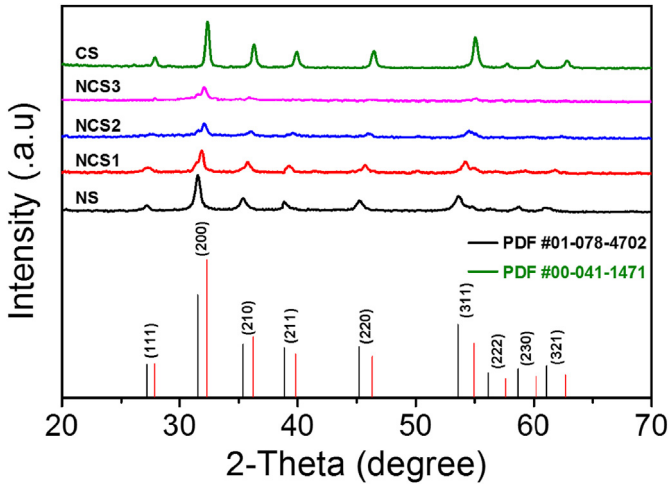

Fig. 2. XRD patterns of the as-synthesized metal sulfides along with the patterns of reference materials of NiS2 (PDF #01-078-4702, black bars) and CoS_2 (PDF #00-041-1471, olive bars).

3. Results and discussion

3.1. Structural and morphological characterization

The crystallization of all synthesized materials was identified by XRD technique. As shown in Fig. 2, the XRD patterns of NS and CS samples could be assigned to NiS_2 (PDF #01-078-4702) and CoS_2 (PDF #00-041-1471), respectively. The observed diffraction peaks of NS (CS) at 27.23 (27.90), 31.56 (32.35), 35.40 (36.31), 38.86 (39.90), 45.26 (46.41), 53.60 (55.07), 56.40 (57.80), 58.72 (60.37) and 61.09 (62.90) are appropriately indexed to the (111), (200), (210), (211), (220), (311), (222), (023) and (321) planes, respectively. The same diffraction planes of NiS_2 and CoS_2 are closely located to each other due to small difference in the ionic radius of Ni^{2+} (0.0069 nm) and Co^{2+} (0.0065 nm). The observed diffraction peaks of mixed NCSs are in the middle of corresponding peaks of NiS_2 and CoS_2, and the majority of them could be deconvoluted to match with that of NiS_2 and CoS_2. This result indicated the mixed NCSs contained both NiS_2 and CoS_2 phases, and thus NiS_2–CoS_2 interphases, which are expected to provide active sites for electrochemical energy storage.

The thermal stability and thermal decomposition processes of as-prepared samples were investigated by TGA technique and the results are shown in Fig. 3. The small mass loss starting at ~80 °C in all samples (*ca.* 1–5 wt%, Fig. 3a) is due to the dehydration. A strong mass loss (*ca.* 13–22 wt%, Fig. 3b–d) occurring at ~400 °C in all Ni-containing samples (NS, NCS1, NCS2, and NCS3) and at ~430 °C in CS sample is due to their thermal decomposition (desulfurization) from MS_2 into MS (M = Ni, Co) [30–32]. Fig. 3B clearly shows that this mass loss increases with increasing Ni:Co molar ratio. In addition, CS sample without Ni is desulfurized at a higher

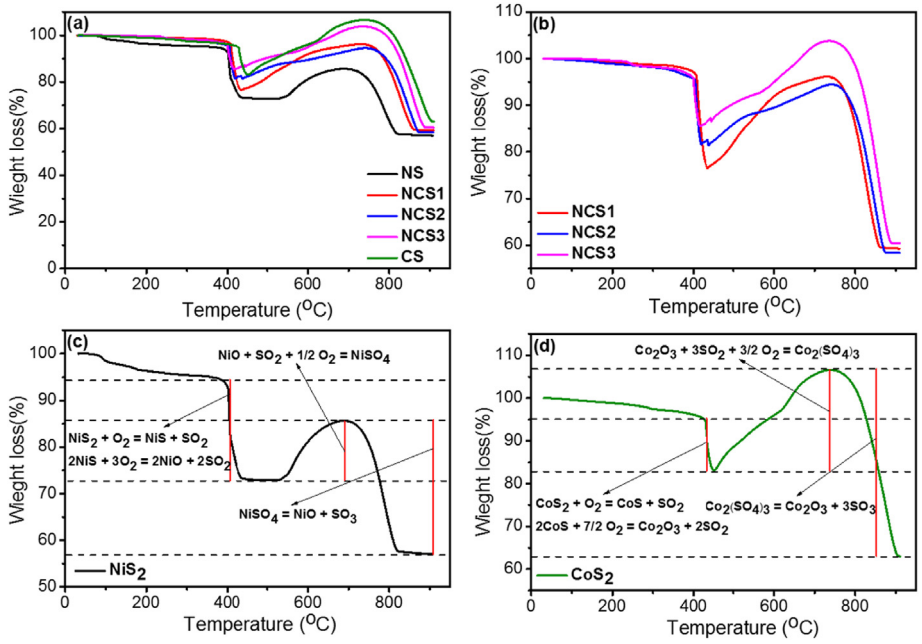

Fig. 3. **(a)** Full-scale TG analysis of all samples; **(b)** TG analysis of mixed NCSs. Thermal decomposition processes of NiS_2 **(c)** and CoS_2 **(d)**.

temperature than all Ni-containing samples (~30 °C higher), indicating that CoS_2 sample is thermally more stable than Ni-containing ones. The resulting MS could be partly oxidized to corresponding oxides (NiO or Co_2O_3). However, this oxidation step was difficult to control, and it is likely possible that not only a single compound exists at this stage of heating. The subsequent and great mass gain is due to the formation of $NiSO_4$ (Fig. 3c), $Co_2(SO_4)_3$ (Fig. 3d) or both (Fig. 3b). Upon heating to ca. 700 °C and above, these sulfates are decomposed into NiO or Co_2O_3, generating sulfur dioxide (SO_2). This step completes at ~810 °C for the NS (Fig. 3c) [31], at ~850 °C for the CS (Fig. 3d) [33], and at ~825–845 °C for the NCSs (Fig. 3b). The residual weight was ~57% for the NS and ~63.1% for the CS, which was agreeing with their expected formula (NiS_2 for NS sample, CoS_2 for CS sample, and mixed NiS_2–CoS_2 for NCS samples).

The morphology of the pristine (NS, CS) and the mixed NCS samples was examined by SEM and TEM techniques and the results are shown in Fig. 4 and Fig. S(1–6). SEM images of NS sample at low- and high magnification (Fig. 4(a-a2)) show that NS sample mainly contains microspheres having a wide range of diameter (*ca.* 100 nm up to 2 μm). These microspheres are very dense and their constituents were difficult to observe even by using TEM (Fig. S6a).

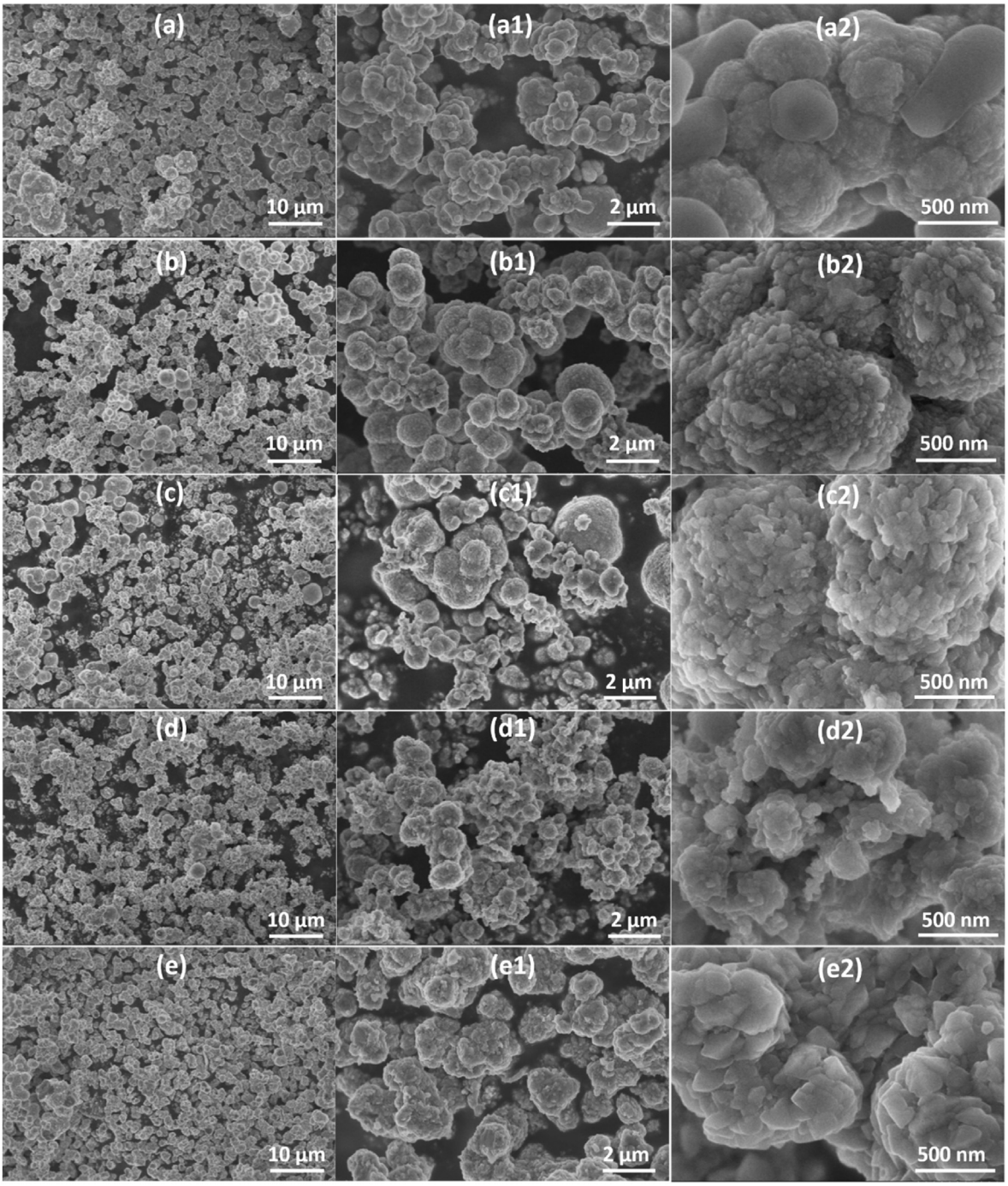

Fig. 4. SEM images of NS (a, a1, a2); NCS1 (b, b1, b2); NCS2 (c, c1, c2); NCS3 (d, d1, d2); and CS (e, e1, e2).

SEM images of NCS samples (Fig. 4(b-d2)) exhibit cauliflower-like microspheres which are nearly equal in size with that of NS sample. These microspheres are formed by assembly of a large amount of primary nanoparticles due to the absence of surfactants, which are clearly confirmed by TEM images (Fig. S6(b-d)). It is observed that with increasing Co content, the microspheres were gradually deformed, and the size of primary particles noticeably increases. Different from pristine NS and CS samples, the presence of NiS_2–CoS_2 interfaces in NCS samples is expected to provide redox-active sites, which are beneficial for charge storage in supercapacitors. Additionally, Fig. S6(b-d) show that among NCSs, NCS1 sample has the smallest size of primary nanoparticles and the least degree of aggregation, which are desired for better contact with electrolyte during charging/discharging. CS sample (Fig. 4(e-e2) and Fig. S6(e)) also contains microspheres but a large portion of them became deformed and had much larger size of primary particles. Overall, mixed NCS samples exhibited smaller size of primary particles, better dispersibility, and higher density of interfacial redox-active sites than the pristine NS and CS ones. Therefore, they are expected to provide smaller electrical resistivity, higher redox current, and subsequently better electrochemical performances.

The chemical composition of materials was analyzed by energy dispersive X-ray spectroscopy (EDS) analysis (Fig. 5 and Fig. S(7–11)). Fig. 5 illustrates the presence of Ni, S in NS sample; Ni, Co, S in mixed NCSs samples; Co, S in CS sample and the absence of other chemical impurities. The Ni:S and Co:S molar ratios of NS (Fig. 5a) and CS (Fig. 5e) materials were 1:1.97 and 1:1.93, respectively. The result is reasonably agreeing with molecular formula AS_2 (A = Ni, Co) and consistent with XRD results. For all mixed NCSs, the Ni:Co:S molar ratio of NCS1, NCS2, NCS3 sample were 0.74:0.26:1.92, 0.49:0.51:1.94, and 0.27:0.73:1.87, respectively. The Ni:Co molar ratio of in all mixed NCSs is also equivalent to Ni^{2+}:Co^{2+} molar ratio of A^{2+} (A = Ni, Co) precursors.

To sum up, the XRD, TGA, SEM, and EDS results confirmed that nickel sulfide, cobalt sulfide, and mixed nickel-cobalt sulfide with high purity have been successfully synthesized. The chemical composition, crystal structure, and morphology were determined by the Ni:Co molar ratio in precursors, which have profound effects on electrochemical properties of the resulting materials.

3.2. Electrochemical characteristics

3.2.1. CV analysis

Fig. 6(a-e) show the CV curves of NS, NCS1, NCS2, NCS3 and CS at different scan rates. In all of these CV curves, a pair of redox peaks appears, which could be attributed to Faradaic reactions of M–S/M–S–OH pairs (M = Ni, Co) [34]. This characteristic indicates that all materials exhibit pseudocapacitor behaviour, and their main mechanism for energy storage is based on redox reactions. Although mixed NCSs simultaneously contain two different M–S bonds (Ni and Co), their Faradaic reactions occur at similar potentials and no redox peak separation was observed. At higher scan rates, the oxidation peaks of all samples shift to higher potentials, whereas the reduction peaks contrarily shift to lower potentials. Simultaneously, both the maximum anodic current (I_{pa}) and the maximum cathodic current (I_{pc}) increase. These indicate that the redox events occurring at the electrode/electrolyte interface are fast, reversible and are only limited by the diffusion of electrolyte ions [35]. At the same scanning rate, the potential at the redox peaks of all mixed NCSs increases as the Ni:Co molar ratio decreases and it was in the potential range of the redox peaks of NS and CS samples. Specifically, the mixed NCS prepared at a Ni:Co molar ratio of 3:1 (NCS1 sample) shows the highest redox current and largest surrounded area of CV curve. It is obviously that the NCS1 sample exhibited the highest capacitance among all prepared samples. The specific capacitance (C_s) of these materials at different scan rates

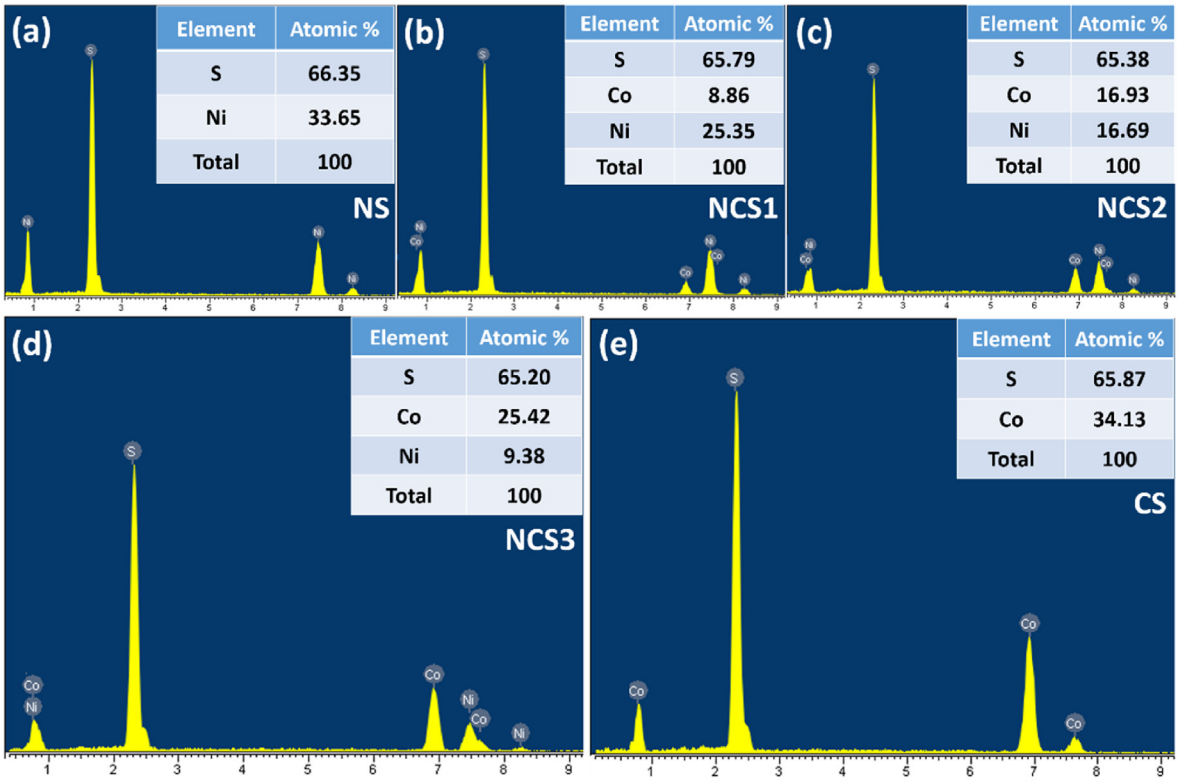

Fig. 5. EDX profiles of NS (a); NCS1 (b); NCS2 (c); NCS3 (d) and CS (e).

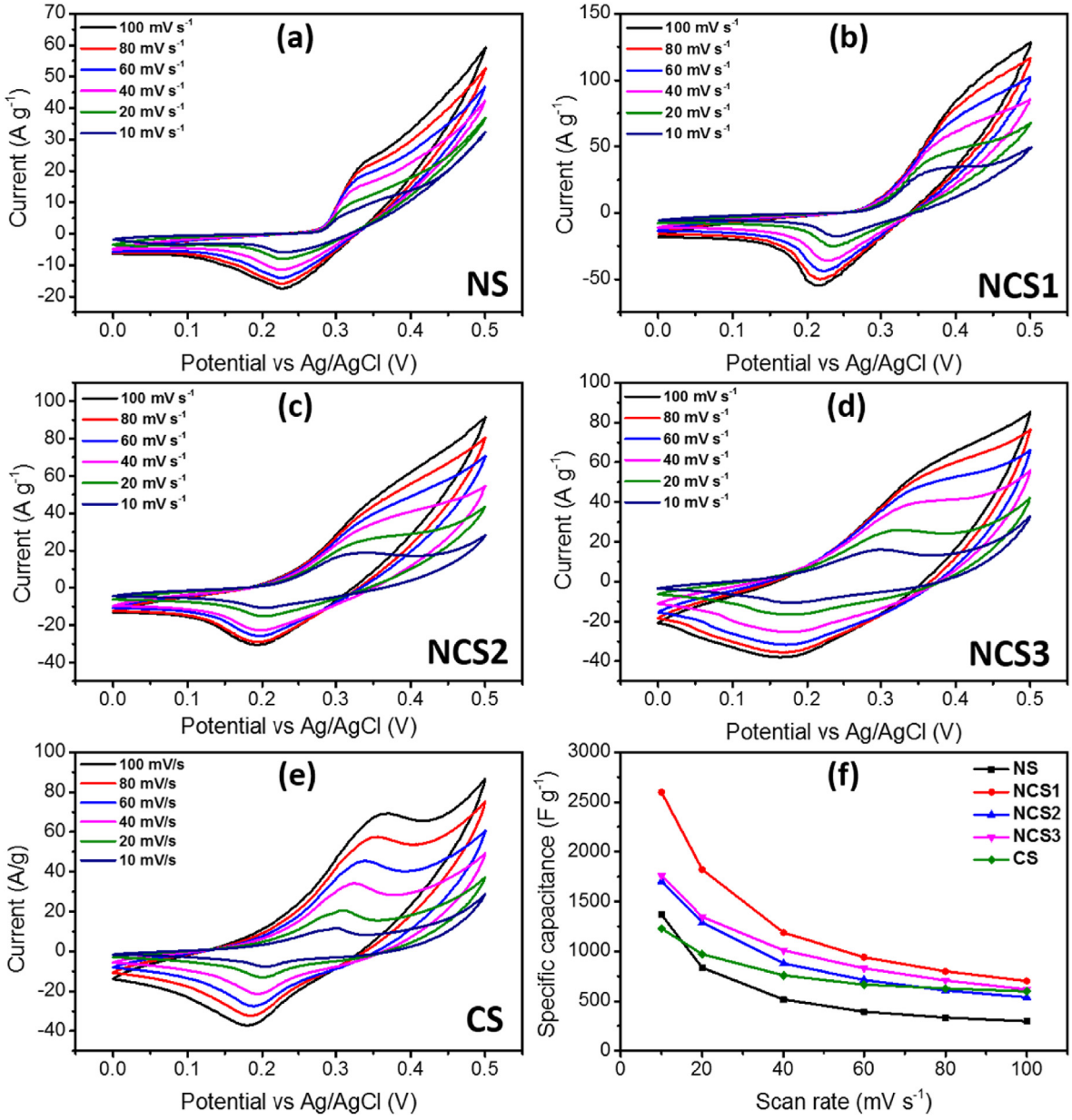

Fig. 6. (**a**–**e**) CV curves of all materials at different scan rate; (**f**) Specific capacitance of all materials at different scan rates.

was calculated and are shown in Fig. 6f and Table S2.

For all materials, when the scan rate decreases, the specific capacitance increases. It was observed that at the same scan rate, the C_s values of all NCS samples are significantly higher than those of the pristine NS or CS ones. The values of C_s obtained at 10 mV s^{-1} and 100 mV s^{-1} for NS, NCS1, NCS2, NCS3 and CS active materials were calculated to be 1369.3/298.3, 2599.6/703.5, 1730.2/538.7, 1760/618.7 and 1230.9/598.4 F g^{-1}, respectively. These C_s values were used to calculate rate capacity, which is considered an important attribution for a supercapacitor electrode material. Within a range of scanning rates, the rate capacity is the ratio between the C_s values at the maximum and the minimum scanning rate. The calculated rate capacities of NS, NCS1, NCS2, NCS3 and CS were 0.22, 0.27, 0.32, 0.35 and 0.49, respectively. Therefore, the addition of Co into NiS_2 not only enhances the C_s value but also increases the rate capacity as compared to NiS_2 sample. This effect suggests a synergistic effect between the faradaic redox reactions of Ni and Co in NCSs.

3.2.2. GCD analysis

To evaluate the *C*s of the obtained mixed nickel-cobalt sulfide, GCD measurements were conducted within the potential range of 0−0.43 V at different current densities from 2 to 10 A g^{-1}. As shown in Fig. 7(a-e), the GCD voltage profiles present voltage plateaus and match well with the peak potentials observed in the CV curves, indicating that the energy storage mechanism of all materials is based on Faradaic reactions. The observed iR drops were very small, implying a high reversibility and Coulombic efficiency of the electrode materials.

The specific capacitance values were calculated based on GCD voltage profiles and are shown in Fig. 7f and Table S3. In all samples, the C_s values decrease when the current density increases. However, the dependence of C_s on the current density is significantly different. Specifically, when the current density increases 5 times

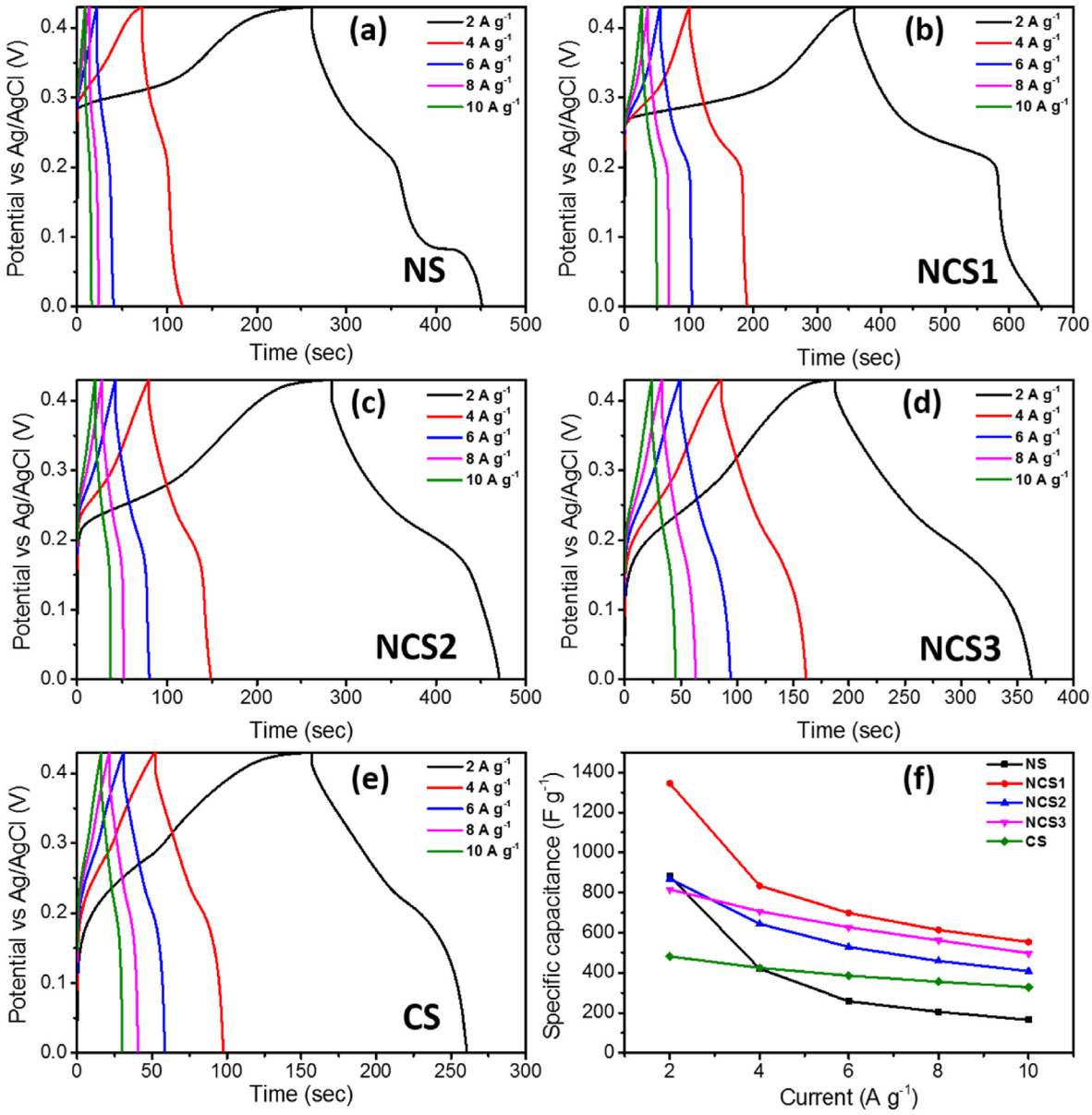

Figure 7. **(a–e)** GCD curves of all electrode materials at different current densities; **(f)** Specific capacitance of all materials at different current density.

Table 2
Comparison of capacitance performance with that of previously reported mixed metal sulfides.

Electrode materials	Method of synthesis	Electrolyte	C_s	Reference
NiS_2	Microwave	3 M KOH	695 F g^{-1} at 1.25 A g^{-1}	[24]
CoS_2 nanowire	Hydrothemal	6 M KOH	828.2 F g^{-1} at 10 mV s^{-1}	[39]
MoS_2 nanosheet	Hydrothemal	6 M KOH	683 F g^{-1} at 1 A g^{-1}	[40]
$Ni_{0.32}Co_{0.68}S_2$		2 M KOH	1698 F g^{-1} at 2 A g^{-1}	[27]
CoS_2@MoS_2	Hydrothemal	2 M KOH	1038 F g^{-1} at 1 A g^{-1}	[36]
Nickel-cobalt sulfides	Electrodeposited	3 M KOH	956.67 F g^{-1} at 2 A g^{-1}	[37]
Ni_3S_4@MoS_2	Hydrothermal	6 M KOH	1440.9 F g^{-1} at 2 A g^{-1}	[38]
NiS_2/CoS_2/N-doped Carbon		6 M KOH	1350 F g^{-1} at 1 A g^{-1}	[26]
NiS/rGO composites	Hydrothermal		905.3 F g^{-1} at 0.5 A g^{-1}	[41]
Nickel sulfides/MoS_2		2 M KOH	757 F g^{-1} at 0.5 A g^{-1}	[42]
NiS_2/ZnS			1198 F g^{-1} at 1 A g^{-1}	[43]
Ni_3S_2@β-NiS			1158 F g^{-1} at 2 A g^{-1}	[44]
NCS1	Solvothermal	3 M KOH	1345 F g^{-1} at 2 A g^{-1}	This work

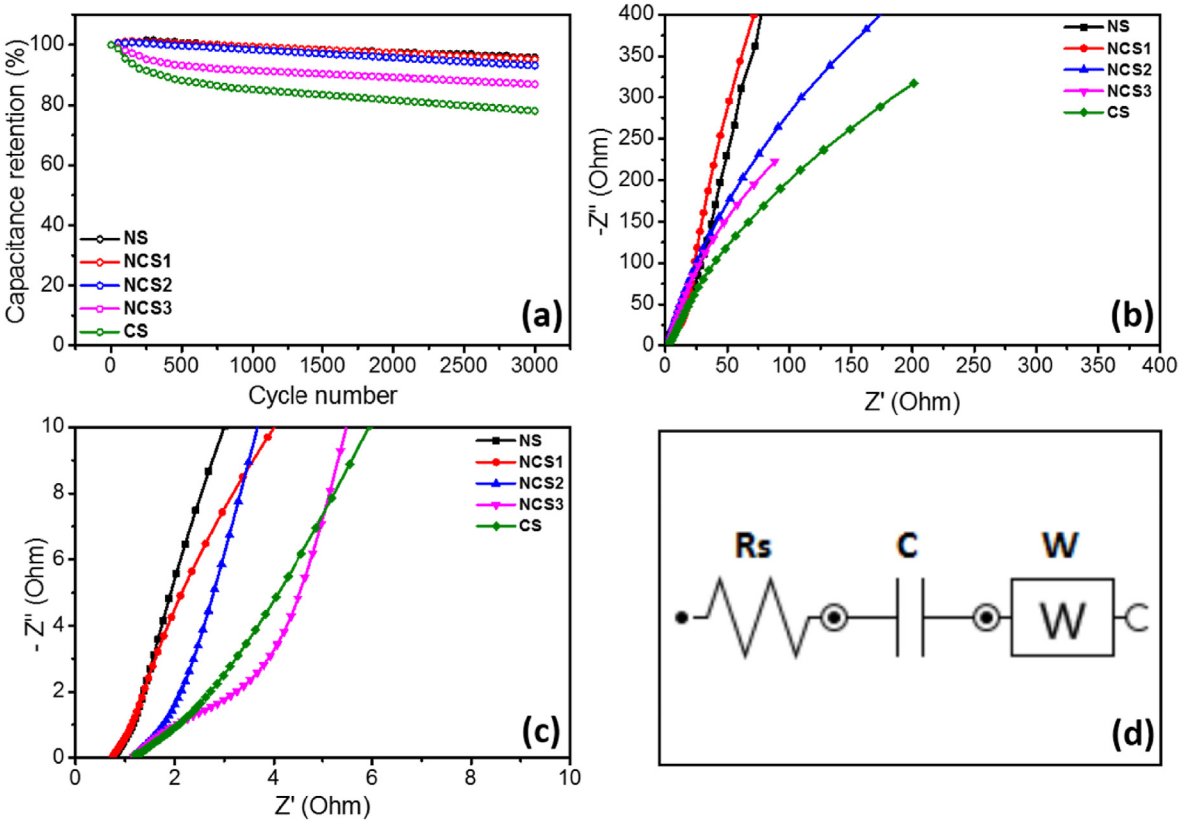

Fig. 8. **(a)** Cycling performance of all materials for 3000 cycles at a current density of 6 A g^{-1}; **(b–c)** Nyquist plots of all materials at all frequency and high-frequency region, respectively; **(d)** Equivalent circuit diagram used for fitting EIS data.

(2–10 A g^{-1}), the C_s decreases 5.34, 2.43, 2.13, 1.64 and 1.47 times with respect to NS, NCS1, NCS2, NCS3 and CS samples. This result indicates that the rate capacity increases in the order of NS < NCS1 < NCS2 < NCS3 < CS. Therefore, controlling the composition of the electrode material is an important factor to change the rate capacity as desired.

Fig. 7f also shows that at the same current density, the C_s of NCS1 is always highest among those of obtained materials. Specifically, at the current density of 2 A g^{-1}, the C_s of NCS1 is 1345 F g^{-1}, much higher than that of NS (881.9 F g^{-1}), NCS2 (868.8 F g^{-1}), NCS3 (815.8 F g^{-1}) and CS (481.6 F g^{-1}). These results match well with the CV results and show a strong evidence of the synergistic effect of Faradaic conversions between M–S/M–S–OH (M = Ni, Co) pairs in mixed NCSs. A similar phenomenon has been also observed in other mixed metal sulfides such as $Ni_{0.32}Co_{0.68}S_2$ [27], CoS_2@MoS_2 [36], nickel-cobalt sulfides [37], and Ni_3S_4@MoS_2 [38]. The C_s of NCS1 is superior or similar to those of many other oxide-based electrodes, as evident in Table 2.

3.2.3. Cycling stability

The cycling performance of all synthesized materials was evaluated by repeating GCD measurement for 3000 cycles at a high current density of 6 A g^{-1} and the result is shown in Fig. 8a. The C_s of NS, NCS1, and NCS2 increased upon cycling, reached the maximum values at *ca.* 150th cycle, and slowly decreased in subsequent cycles. Meanwhile, the C_s of NCS3 and CS reached the maximum values at the first cycle and immediately decreased in subsequent cycles. This feature indicates that mixed NCSs with high nickel content require longer time to gain full activation of electrode surface. After 3000 consecutive cycles, the capacitance retention decreases in the order of NS (96%) > NCS1 (95%) > NCS2 (93%) > NCS3 (87%) > CS (78%). Note that the Ni:Co molar ratio also decreases following that order. These values indicate that the cycling performance of the synthesized sulfides decreased with increasing Co content in mixed NCSs. Among all samples, the NCS1 not only exhibited immediate activation of electrode surface but also retained high capacitance after 3000 cycles.

3.2.4. EIS analysis

EIS measurements were performed in order to analyze various parameters related to the reaction kinetics at the electrode/electrolyte interface. The Nyquist plots of all samples are presented in Fig. 8b-c, the equivalent circuit diagram used for fitting EIS data is shown in Fig. 8d, and the corresponding fitting parameters are given in Table S4. As shown in Fig. 8c and Table S4, the equivalent series resistance (R_s) of all materials is small and increases when mass ratio of cobalt increases. This result indicates that the conductivity of electrode materials decreases with the increasing cobalt content in the materials. The diffusive resistance of OH^- electrolyte ions is evaluated through the slope of the plots in the low frequency region [45], Fig. 8b-c show that the higher the cobalt content in the materials, the higher the OH^- diffusive resistance. Impressively, the Nyquist plots of NS and NCS1 in the low-frequency region show a nearly vertical line, indicating a high electron mobility and ideal battery-like behaviour [46,47]. These analyses indicate that NS and NCS1 had lower resistance and faster redox reaction kinetics than those other mixed NCSs.

4. Conclusions

In summary, we have successfully prepared mixed NCSs by a facile solvothermal route and examined them as a high-

performance electrode material for supercapacitor. The mixed NCSs showed enhanced electrochemical performances than those of the pristine NiS_2 and CoS_2 ones, which signified the synergistic effect between Ni and Co in mixed NCSs. The smaller particle size and the presence of NiS_2–CoS_2 interfaces in mixed NCOs was found to reduce diffusion resistance, leading to high-capacitance and long-life performance for supercapacitor. In particular, the mixed NCS1 exhibited an impressive C_s of 2599.6 F g^{-1} at 10 mV s^{-1} (or 1345 F g^{-1} at 2 A g^{-1}) and an excellent capacitance retention of 95% after 3000 charge-discharge cycles at 6 A g^{-1}. The combination and tuning of multiple metallic sulphides proposed in this work could provide a feasible strategy for developing novel electrode materials for supercapacitor.

Declaration of competing interest

There are no conflicts of interest to declare.

CRediT authorship contribution statement

To Van Nguyen: Conceptualization, Data curation, Formal analysis, Investigation, Methodology, Supervision, Validation, Visualization, Writing - original draft, Writing - review & editing. **Luong Trung Son:** Formal analysis, Investigation, Methodology, Validation, Writing - review & editing. **Pham Manh Thao:** Formal analysis, Investigation, Methodology, Validation, Writing - review & editing. **Le The Son:** Formal analysis, Investigation, Methodology, Validation, Writing - review & editing. **Doan Tien Phat:** Formal analysis, Investigation, Methodology, Validation, Writing - review & editing. **Ngo Thi Lan:** Formal analysis, Investigation, Methodology, Validation, Writing - review & editing. **Nguyen Van Nghia:** Formal analysis, Investigation, Methodology, Validation, Writing - review & editing. **Tran Viet Thu:** Conceptualization, Data curation, Formal analysis, Funding acquisition, Methodology, Project administration, Resources, Supervision, Visualization, Writing - original draft, Writing - review & editing.

Appendix A. Supplementary data

Supplementary data to this article can be found online at https://doi.org/10.1016/j.jallcom.2020.154921.

References

[1] S. Xie, J. Gou, Facile synthesis of $Ni_2P/Ni_{12}P_5$ composite as long-life electrode material for hybrid supercapacitor, J. Alloys Compd. 713 (2017) 10–17.
[2] H. Yin, Z. Tang, Ultrathin two-dimensional layered metal hydroxides: an emerging platform for advanced catalysis, energy conversion and storage, Chem. Soc. Rev. 45 (18) (2016) 4873–4891.
[3] Z. Wang, et al., Long cyclic life in manganese oxide-based electrodes, ACS Appl. Mater. Interfac. (2016) 8.
[4] Y. Guo, et al., Hierarchical tubular structures composed of Mn-based mixed metal oxide nanoflakes with enhanced electrochemical properties, Adv. Funct. Mater. (2015) 25, https://doi.org/10.1002/adfm.201501974.
[5] J. Zhao, et al., Flexible electronics: hierarchical NiMn layered double hydroxide/carbon nanotubes architecture with superb energy density for flexible supercapacitors (adv. Funct. Mater. 20/2014), Adv. Funct. Mater. (2014) 24.
[6] J.M. Tarascon, M. Armand, Issues and challenges facing rechargeable lithium batteries, Nature 414 (2001) 359–367.
[7] S. Ahmed, A. Ahmed, M. Rafat, Supercapacitor performance of activated carbon derived from rotten carrot in aqueous, organic and ionic liquid based electrolytes, J. Saudi Chem. Soc. 22 (8) (2018) 993–1002.
[8] J. Huang, et al., 3D honeycomb-like carbon foam synthesized with biomass buckwheat flour for high-performance supercapacitor electrodes, Chem. Commun. 55 (62) (2019) 9168–9171.
[9] L.F. Aval, M. Ghoranneviss, G.B. Pour, High-performance supercapacitors based on the carbon nanotubes, graphene and graphite nanoparticles electrodes, Heliyon 4 (11) (2018) e00862.
[10] W. Yang, et al., Graphene in supercapacitor applications, Curr. Opin. Colloid Interface Sci. 20 (5) (2015) 416–428.
[11] T.V. Thu, et al., Graphene-$MnFe_2O_4$-polypyrrole ternary hybrids with synergistic effect for supercapacitor electrode, Electrochem. Acta. 314 (2019) 151–160.
[12] Poonam, et al., Review of supercapacitors: materials and devices, J. Energy Stor. 21 (2019) 801–825.
[13] M. Huang, et al., MnO_2-based nanostructures for high-performance supercapacitors, J. Mater. Chem. 3 (43) (2015) 21380–21423.
[14] K.-y Liu, et al., Charge-discharge process of MnO_2 supercapacitor, Trans. Nonferrous Metals Soc. China 17 (3) (2007) 649–653.
[15] Y. Li, et al., Review and prospect of $NiCo_2O_4$-based composite materials for supercapacitor electrodes, J. Energy Chem. 31 (2019) 54–78.
[16] A.K. Yedluri, H.-J. Kim, Enhanced electrochemical performance of nanoplate nickel cobaltite ($NiCo_2O_4$) supercapacitor applications, RSC Adv. 9 (2) (2019) 1115–1122.
[17] W. Zhibin, Y. Zhu, X. Ji, $NiCo_2O_4$-based materials for electrochemical supercapacitors, J. Mater. Chem. (2014) 2.
[18] Z. Su, et al., Scalable fabrication of MnO2 nanostructure deposited on free-standing Ni nanocone arrays for ultrathin, flexible, high-performance micro-supercapacitor, Energy Environ. Sci. 7 (8) (2014) 2652–2659.
[19] J. Duay, et al., Self-limiting electrodeposition of hierarchical MnO_2 and $M(OH)_2/MnO_2$ nanofibril/nanowires: mechanism and supercapacitor properties, ACS Nano 7 (2) (2013) 1200–1214.
[20] B. Wang, et al., Green synthesis of NiO nanobelts with exceptional pseudocapacitive properties, Adv. Energy Mater. (2012) 2.
[21] J. Xiao, et al., Design hierarchical electrodes with highly conductive $NiCo_2S_4$ nanotube Arrays grown on carbon fiber paper for high-performance pseudocapacitors, Nano Lett. (2014) 14.
[22] H. Chen, et al., Highly conductive $NiCo_2S_4$ urchin-like nanostructures for high-rate pseudocapacitors. Nanoscale, 2013, p. 5.
[23] J.-C. Xing, et al., Fabrication and shape evolution of CoS_2 octahedrons for application in supercapacitors, Electrochem. Acta 136 (2014) 550–556.
[24] H. Pang, et al., Microwave-assisted synthesis of NiS_2 nanostructures for supercapacitors and cocatalytic enhancing photocatalytic H_2 production, Sci. Rep. 4 (2014) 3577.
[25] L. Wang, et al., Supercapacitor performances of the MoS_2/CoS_2 nanotube Arrays in situ grown on Ti plate, J. Phys. Chem. C (2017) 121.
[26] H. Liu, et al., Metal-Organic frameworks-derived NiS_2/CoS_2/N-doped carbon composites as electrode materials for asymmetric supercapacitor, ChemElectroChem 6 (2019) 3764–3773.
[27] L. Jin, et al., Synthesis of mesoporous CoS_2 and $Ni_xCo_{1-x}S_2$ with superior supercapacitive performance using a facile solid-phase sulfurization, ACS Appl. Mater. Interfaces 9 (42) (2017) 36837–36848.
[28] X. Li, et al., Template-free solvothermal synthesis of NiS_2 microspheres on graphene sheets for high-performance supercapacitors, Mater. Lett. 139 (2015) 81–85.
[29] B. Wang, et al., Solvothermal synthesis of CoS_2–graphene nanocomposite material for high-performance supercapacitors, J. Mater. Chem. 22 (2012) 15750–15756.
[30] J. Tang, et al., A free template strategy for the synthesis of CoS_2-reduced graphene oxide nanocomposite with enhanced electrode performance for supercapacitors, Ceram. Int. 40 (10, Part A) (2014) 15411–15419.
[31] S.-L. Yang, et al., Monodisperse cubic pyrite NiS_2 dodecahedrons and microspheres synthesized by a solvothermal process in a mixed solvent: thermal stability and magnetic properties, CrystEngComm 11 (7) (2009) 1383–1390.
[32] B. Wang, et al., Solvothermal synthesis of CoS_2–graphene nanocomposite material for high-performance supercapacitors, J. Mater. Chem. 22 (31) (2012) 15750–15756.
[33] H. Gu, et al., Electrospun carbon nanofiber@CoS2 core/sheath hybrid as an efficient all-pH hydrogen evolution electrocatalyst, Inorgan. Chem. Front. 3 (10) (2016) 1280–1288.
[34] T. Chen, et al., Synergistic effect of cobalt and nickel on the superior electrochemical performances of rGO anchored nickel cobalt binary sulfides, Electrochem. Acta. 212 (2016) 294–302.
[35] P. Xu, et al., Carbon nanotube fiber based stretchable wire-shaped supercapacitors, Adv. Energy Mater. (2014) 4.
[36] F. Huang, et al., One-step hydrothermal synthesis of a CoS_2@MoS_2 nanocomposite for high-performance supercapacitors, J. Alloys Compd. 742 (2018) 844–851.
[37] S. Xu, et al., One-step electrodeposition of nickel cobalt sulfide nanosheets on Ni nanowire film for hybrid supercapacitor, Electrochem. Acta. 259 (2018) 617–625.
[38] F. Huang, et al., One-step hydrothermal synthesis of Ni_3S_4@MoS_2 nanosheet on carbon fiber paper as a binder-free anode for supercapacitor, J. Mater. Sci. Mater. Electron. 28 (2017) 1–8.
[39] R. Ren, et al., Metallic CoS_2 nanowire electrodes for high cycling performance supercapacitors, Nanotechnology 26 (2015), 494001.
[40] Y.-P. Gao, et al., MoS_2 nanosheets assembling three-dimensional nanospheres for enhanced-performance supercapacitor, J. Alloys Compd. 741 (2018) 174–181.
[41] J. Yang, et al., Electrochemical performances investigation of NiS/rGO composite as electrode material for supercapacitors, Nanomater. Energy 5 (2014) 74–81.
[42] X. Yang, L. Zhao, J. Lian, Arrays of hierarchical nickel sulfides/MoS_2 nanosheets supported on carbon nanotubes backbone as advanced anode materials for asymmetric supercapacitor, J. Power Sources 343 (2017) 373–382.
[43] G.-C. Li, et al., MOF-derived self-sacrificing route to hollow NiS_2/ZnS

nanospheres for high performance supercapacitors, RSC Adv. 6 (105) (2016) 103517−103522.
[44] W. Li, et al., Single-crystal β-NiS nanorod arrays with a hollow-structured Ni_3S_2 framework for supercapacitor applications, J. Mater. Chem. 4 (20) (2016) 7700−7709.
[45] C. Wei, et al., Soft-template hydrothermal systhesis of nanostructured copper(II) tungstate cubes for electrochemical charge storage application, Electrochem. Acta. 220 (2016) 156−163.
[46] X. Wang, et al., Achieving high rate performance in layered hydroxide supercapacitor electrodes, Adv. Energy Mater. (2014) 4.
[47] J. Gou, Ni_2P/NiS_2 composite with phase boundaries as high-performance electrode material for supercapacitor, J. Electrochem. Soc. 164 (2017) A2956−A2961.